Computational Materials Science 197 (2021) 110635

Contents lists available at ScienceDirect

Computational Materials Science

journal homepage: www.elsevier.com/locate/commatsci

Atomistic study of shock Hugoniot in columnar nanocrystalline copper

Jianqiao Hu [a,b,*], Zhen Chen [c]

[a] State Key Laboratory of Nonlinear Mechanics, Institute of Mechanics, Chinese Academy of Sciences, Beijing 100190, PR China
[b] School of Engineering Science, University of Chinese Academy of Sciences, Beijing 100049, PR China
[c] College of Engineering, University of Missouri, Columbia, MO 65211, USA

ARTICLE INFO

Keywords:
Shock Hugoniot
Molecular dynamics
Columnar nanocrystal
Size effect
Shielding effect

ABSTRACT

Understanding the shock behavior of polycrystals is challenging due to the effects of grain size, defect, and orientation. In this study, we focus on the grain size and defect effects on the shock Hugoniot of polycrystals using columnar nanocrystalline copper. The dominant deformation mechanism is clarified under the impact velocities ranging from 300 m/s to 1200 m/s. The main findings from this study are as follows. The shock Hugoniot relation between pressure and specific volume has no clear dependence on the grain size, whereas the corresponding Hugoniot shear stress exhibits a grain size dependence. The primary defects of shock plasticity change from dislocation to stacking fault and finally twinning with the increase of impact velocity. As the impact velocity exceeds 1000 m/s, the shielding effect becomes prominent as a result of the defect formation on the parallel slip planes within a grain.

1. Introduction

Shock loading has long been used to study the transient properties of metallic materials [1–3], which is of great significance in many engineering applications such as high-speed machining and impact. When the shock pressure exceeds the Hugoniot elastic limit (HEL, above which plasticity occurs), various types of defects would be generated. The defect evolution differs from that in the quasi-static plastic deformation as a result of the rate-dependent effect under shock pressure. Various kinds of experiments [4–6] have provided a large amount of Hugoniot data under a wide range of shock pressure. Among those experimental techniques, the laser-pulse loading, as first demonstrated by Askaryon and Morez [7] in 1963, serves as an effective technique to generate extremely high-pressure shock pulses. By carrying out the laser-induced shock loading on the single crystalline copper, Meyers et al. [8] concluded that the dominant defects were pressure-dependent, namely, dislocation cells at the pressure level of 12 GPa to 20GPa, twining and stacking fault at 40 GPa and micro-twinning at 55 ~ 60 GPa. Other studies with the laser shock experiments demonstrated the effects of crystal orientation [9,10] and pulse duration [11]. In the shock experiments, however, the real-time observation is challenging because the defects generally evolve within a short period of time. As a result, the analysis of the primary defects is often inferred from the recovered sample's microstructure.

Numerical modeling and evaluation can provide the real-time details of the shock plasticity [12–14] and bridge the connection between the shock Hugoniot and primary defects under different levels of shock pulses. Using molecular dynamics (MD) simulations, Cao et al. [15] studied the shock-induced plasticity in the single crystalline copper and found the density of defects is much larger than that observed in the experiments [16]. They proposed one possible reason, namely, the defects evaluated from the experimental data are based on the recovered samples, in which most of the defects are possibly annealed out. The MD simulations of perfect single crystals have revealed the relation between dislocation nucleation and material parameters [17] and the effect of the crystal orientation on dislocation nucleation and multiplication [18,19]. In these single crystals without initial defects, the shock plasticity is initiated by the nucleation of different kinds of resulting defects. In contrast, for samples containing initial defects, the pre-existing microstructural characteristics may also affect the transient response of metals [20,21]. By introducing voids of different sizes in the perfect crystals, Takahiro [22] showed that the HEL drastically decreases as the void size increases.

For the polycrystalline metals, the grain boundaries (GBs) also serve as the primary initial defect sources. Comparing with single crystals, the existence of GBs changes the critical shock velocity at HEL [23]. Numerous MD investigations were carried out to study the GB effect on the shock response of nanocrystalline (NC) materials, including the

* Corresponding author at: State Key Laboratory of Nonlinear Mechanics, Institute of Mechanics, Chinese Academy of Sciences, Beijing 100190, PR China.
E-mail address: jianqiaohu@imech.ac.cn (J. Hu).

https://doi.org/10.1016/j.commatsci.2021.110635
Received 15 March 2021; Received in revised form 19 May 2021; Accepted 1 June 2021
Available online 10 June 2021
0927-0256/© 2021 Elsevier B.V. All rights reserved.

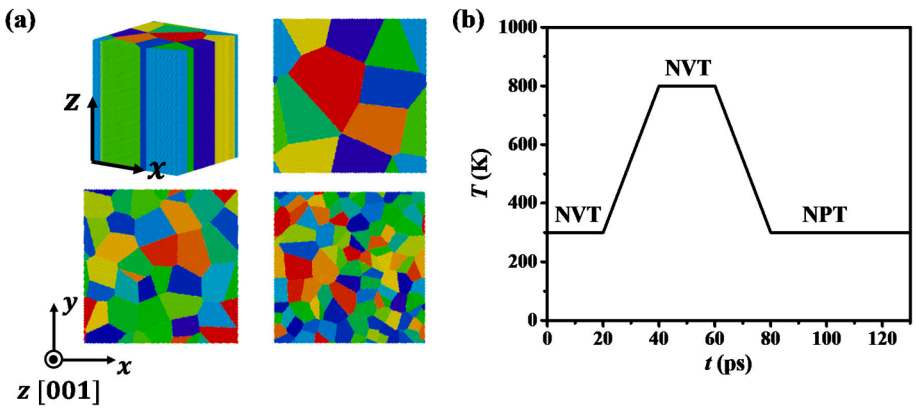

Fig. 1. (a) Schematic diagram of columnar NC copper; (b) A five-stage annealing procedure was performed to relax the nanocrystal.

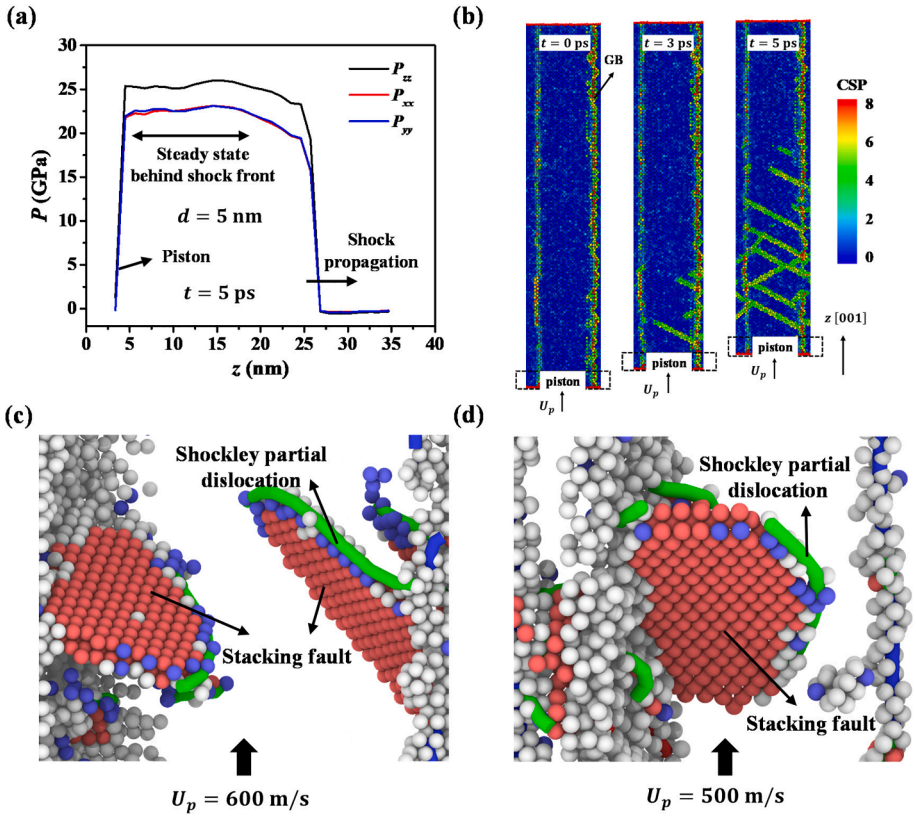

Fig. 2. (a) Typical shock pressure profiles along the loading and transverse directions at the time of 5 ps for the NC copper under an impact velocity of 600 m/s. (b) Visualization of corresponding defects by CSP in a columnar grain. The dominant defects at the time of 2 ps under the impact velocities of (c) 600 m/s and (d) 500 m/s, respectively.

ultrahigh strength and related defects behind the shock front [24], the void nucleation and evolution in the spalling process [25,26], and the effect of grain size and orientation [27]. For the NC metals with randomly distributed grains, however, it is challenging to understand the individual role of GBs because the grain orientation also affects the shock plasticity. By preparing an idealized hexagonal columnar nanocrystal with the same grain orientation along the columnar axis, Luo et al. [28] studied the anisotropic flow stress and spall strength of the NC copper with specific grain size. Although the anisotropic shock response could be related to the grain orientation, the individual effect of grain size remains to be clarified in nanocrystals subjected to different levels of impact.

Motivated by the above issue, we first numerically fabricated the columnar NC copper of different grain sizes for which all grains have the same orientation along the impact direction. Using MD simulations, we then elucidated the effect of grain size on the shock Hugoniot by analyzing the shock response and the evolution of defects. The remaining part of the paper is organized as follows. The MD methodology and model description are presented in section 2. The simulation results, including the shock pressure and the shear stress at Hugoniot state, are discussed, and the defect evolution during impact is analyzed in section 3. Finally, the concluding remarks are given in section 4.

2. Methodology and model description

In this study, MD simulations are performed using the Large-scale Atomic/Molecular Massively Parallel Simulator [29]. To investigate the role of GBs and eliminate the effect of grain orientation, we

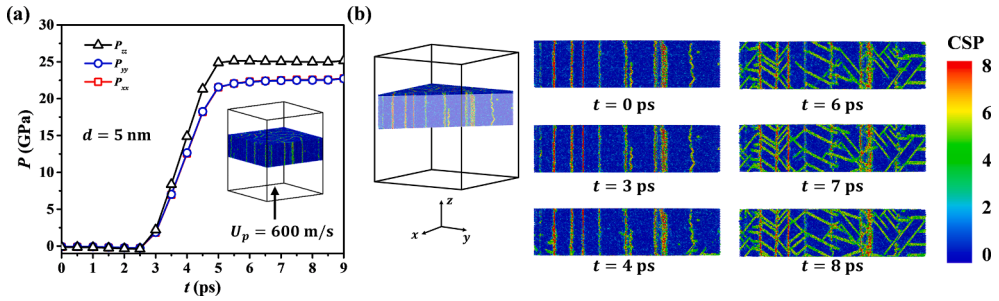

Fig. 3. (a) Evolution of pressures in the RVE; (b) Snapshots of atomic CSP in the cross-section of the RVE in which the shock wave propagates from the bottom to top.

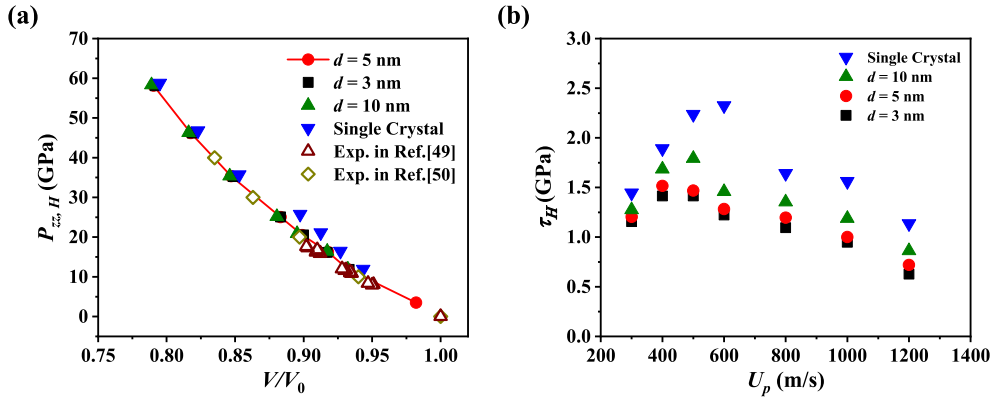

Fig. 4. (a) Shock pressure versus specific volume in columnar NC copper. (b) Shear stress at Hugoniot state under various piston velocities.

fabricated a series of columnar nanocrystals with the same grain orientation along the columnar axis, as illustrated in Fig. 1(a). The nanocrystals with grain sizes varying from 3 nm to 10 nm were constructed with the Voronoi tessellation method using Atomsk [30]. In the columnar nanocrystal, all the grains have the [0 0 1]-orientation along the z-direction, and each grain rotates around the z-axis with a random angle. The size of box cell is 30 nm × 30 nm in the x-y section and 100a along the z-direction with a being the lattice constant 0.3615 nm. For comparison, single-crystalline (SC) copper is fabricated with a dimension of 80a × 80a × 100a along x-[0 0 1], y-[0 1 0], and z-[0 0 1] crystal orientations, respectively. It has been confirmed [15] that this dimension is sufficiently large to obtain the shock Hugoniot. The interaction among copper atoms is described by the embedded atom method (EAM) potential [31]. This potential is widely used to simulate the transient responses of copper, such as the strain rate effect of single crystals with initial defects [32], the shock responses of single crystals [33,34], and the shock-induced melting of single crystals at extremely high pressures [35].

Since the residual stresses would be artificially introduced in the NC copper by the Voronoi construction, an annealing procedure is performed to eliminate the residual stresses before shock loading. As shown in Fig. 1(b), a five-stage procedure [36,37] was adopted to anneal the NC copper with periodic boundary conditions employed along all three axes. First, the NC sample was thermally equilibrated using the NVT ensemble (constant volume and temperature) at 300 K for 20 ps. Second, the sample was gradually heated up to 800 K at constant volume for 20 ps. Then, the sample was thermalized at 800 K in the NVT ensemble during the third stage. In the fourth stage, the sample was cooled down to 300 K in 20 ps, and finally kept equilibrated at 300 K and zero pressure in the NPT ensemble (constant pressure and temperature) for 50 ps.

After the initial atomic configuration was fabricated as above, the boundary condition in the z-direction (i.e., the shock loading direction) was changed to the free surface while the other two directions remained periodic. The atomic model was further relaxed in the NPT ensemble with the temperature of 300 K and the transverse pressure of 0 GPa for 50 ps. The bottom 1 nm of the sample was set as a rigid piston, which impacts the sample on a stationary infinite mass wall. The atoms in the piston were assigned a particle velocity U_p from 300 m/s to 1200 m/s along the z-direction. The NVE ensemble was adopted for the shock simulations, and the time step was chosen to be 1 fs (fs). The simulation cell was divided into fine bins along the shock direction (1D binning analysis) because the heterogeneities in the transverse directions were neglected. A slice with a thickness of 10 nm (i.e., located between 15 nm and 25 nm in the z-axis) was selected as a representative volume element (RVE) to record the shock Hugoniot and microstructure evolution (e.g., dislocations and stacking fault).

In the analysis, the stress tensor of the RVE was calculated as the volumetric average of the atomic stresses derived from the virial theorem [38], as used in previous MD simulations [39,40]. The pressure $P_{zz,H}$, the shear stress τ_H and the specific volume V/V_0 at the Hugoniot state were obtained in the RVE, which is essentially the same as the previous method of averaging the stresses of the bins [41]. For the analysis of microstructure, the dislocation extraction algorithm (DXA) [42] was used to track dislocations, and the common neighbor analysis (CNA) method [43] was adopted to identify the atomic structures. The open-source software OVITO [44] was utilized to visualize the microstructures. The dislocation density is determined by dividing the total length of the dislocation lines in the RVE by RVE's volume. The shear stress is defined as $\tau = -\frac{1}{2}\left[\sigma_{zz} - \left(\sigma_{xx} + \sigma_{yy}\right)/2\right]$ and the pressure along the load direction as $P_{zz} = -\sigma_{zz}$.

3. Results and analysis

3.1. Wave profile and shock Hugoniot

Fig. 2(a) presents a typical shock wave profile for the NC copper with a grain size of 5 nm. The pressures are evaluated by the 1D binning

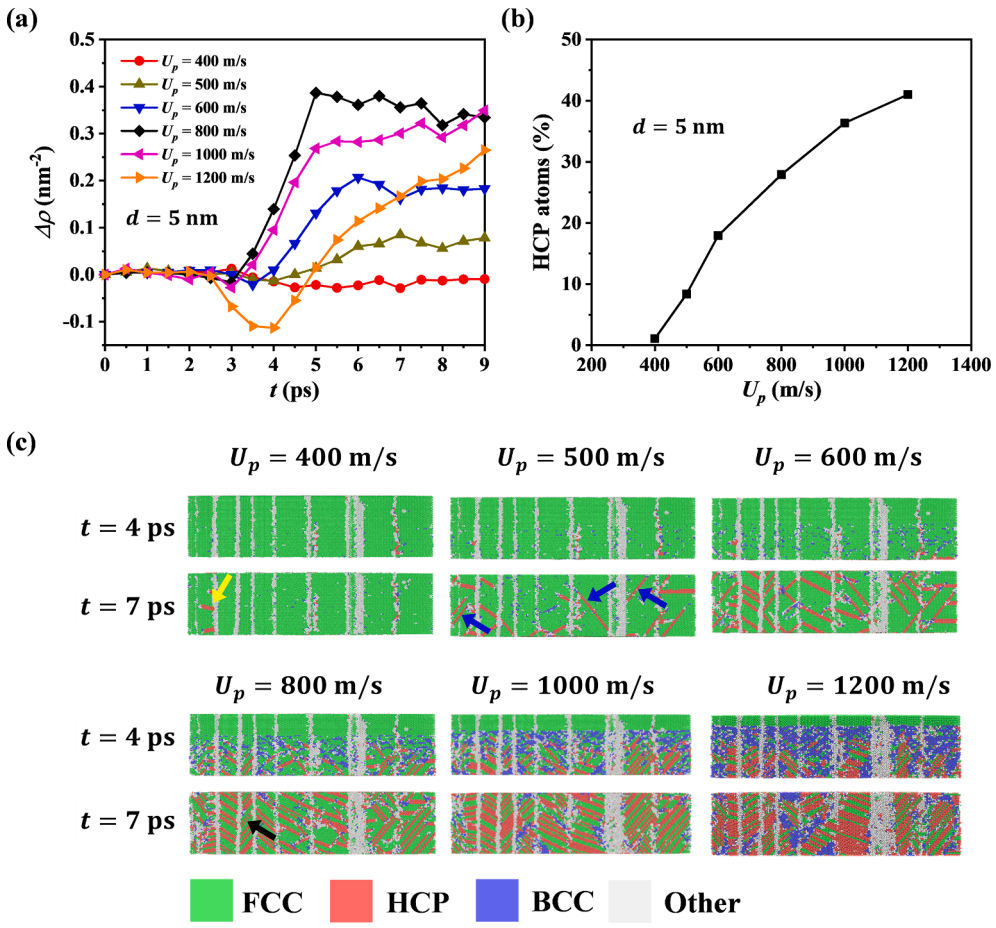

Fig. 5. (a) Dislocation density as a function of shock time in the NC copper with grain size of 5 nm, (b) the percentage of HCP atoms in the RVE at the Hugoniot state. (c) The structure evolution in the RVE based on CNA.

analysis from the snapshot of MD simulations at 5 ps under the impact velocity of 600 m/s. Consistent with the shock wave profile observed previously [45], the shock wave propagates along the loading direction with much faster velocity U_s, triggering the sharp increase of pressures along both the loading and transverse directions at the shock front. Here, the velocity of the shock wave U_s is calculated from the time difference of the shock front at different locations, which yields ~4700 m/s. The pressures remain stable eventually in the deformed region behind the shock front (i.e., the steady-state region).

Correspondingly, the evolution of defects inside a columnar grain is illustrated in Fig. 2(b). The atoms are colored according to their centro-symmetry parameters (CSP), and a higher atomistic CSP generally indicates the existence of defects, e.g., GB, dislocation, and stacking fault. The evolution of defects can be clarified as the shock wave propagates due to the large length of the columnar grain along shock direction. The shock-induced plasticity has emerged in the NC copper atU_p = 500 m/s (see Fig. 2(d)), while no plasticity occurs in the SC copper at$U_p \leq$~750 m/s [46]. As compared with the SC sample, the GBs in the NC copper act as the origin of plasticity, reducing the critical impact velocity at the HEL. At the impact velocity of 600 m/s, the dominant defects are Shockley partial dislocations and the stacking faults, as shown in Fig. 2 (c). Similar shock plasticity can also be observed at the velocity of 500 m/s, see Fig. 2(d). The dislocation nucleates from the GBs and slips across the grain as the piston pushes forward. At the same time, the stacking faults are also generated and bounded by the Shockley partial dislocations. These defects cannot generally penetrate the GB (see Fig. 2 (b)) when they encounter the GB on the other side, and new defects continue to form at the GB around the shock front.

As the shock wave propagates, the pressure in the fully deformed region becomes stable, achieving the Hugoniot state. As shown in Fig. 3 (a), the evolution of pressures in the RVE is presented as the shock time advances. The pressures first increase as the shock precursor reaches the RVE and then remain stable as the RVE is fully deformed. The transverse pressures in the x and y directions exhibit little difference, whereas the pressure along the shock direction is higher than the transverse ones. This result differs from that in the dislocation dynamics (DD) study [47], where the hydrostatic pressure condition without shear stress is finally achieved. The difference may be due to the artificially introduced dislocation sources in the DD simulation. As a result, the shear component can be fully released by dislocation plasticity in the DD study. However, previous MD simulations with a much longer shock time for SC copper at $U_p = 750$ m/s [48] and the shock response of nano-twinned NC copper at $U_p = 600$ m/s [41] have confirmed the existence of shear stress at the Hugoniot state.

The corresponding snapshots of the atomic structures at different shock times are illustrated in Fig. 3(b). At the initial stage (i.e., $t = 3$ ps), although the pressure increased in all three directions, we did not observe apparent newly-formed defects. It is because the shear stress is small at this time, and the new defects cannot be activated. As the shock wave advances ($t = 4$ ps), the shear stress increases, and the new defects emerge from the GBs. Subsequently, numerous defects form in the grains and remain relatively stable. For the RVE considered here, the shock pressures increase to the stable state after ~5 ps. Note that a faster piston velocity U_p can generate a higher shock velocity U_s, advancing the stabilization time in the RVE.

Next, we present the effect of grain size on the shock Hugoniot of the NC copper at the impact velocities from 300 m/s to 1200 m/s, as shown in Fig. 4(a). The results obtained by the MD simulations are consistent

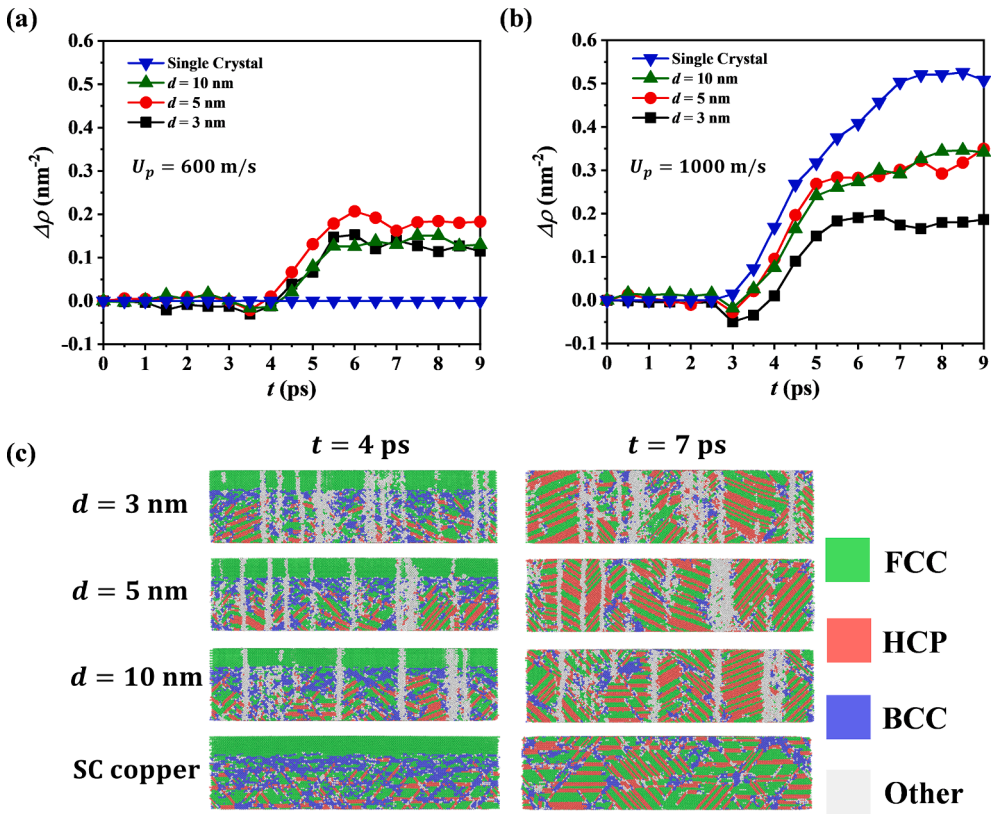

Fig. 6. Evolution of dislocation density in the SC and NC copper with the piston velocities of (a) 600 m/s and (b) 1000 m/s, respectively. (c) The CNA of atoms in the RVE at U_p = 1000 m/s.

with the experimental observations [49,50]. For the nanocrystals studied here, the Hugoniot pressure shows no clear dependence on the grain size, which indicates to some extent that nanocrystals with different grain sizes follow the same Hugoniot relationship under impact loading. The shock experiments also provide the grain size-insensitive Hugoniot pressure. Particularly, for SC copper at the specific volume V/V_0 = 0.9, the shock Hugoniot slightly departs from the NC samples and experimental data. In this case, no plasticity was generated in the SC copper because the critical shock velocity for the HEL is higher in the SC copper than in the NC copper.

Although the NC copper samples of different grain sizes follow a unified Hugoniot relation in the *P-V* space, the corresponding Hugoniot shear stresses exhibit a clear grain size dependence, as shown in Fig. 4 (b). Two primary features can be observed in the variation of Hugoniot shear stress with the change in impact velocity and grain size. First, the larger the grain size, the higher the shear stress. This grain size dependence is consistent with the reverse Hall-Petch effect in the MD simulations of uniaxial tension [51] that the strength for nanocrystalline copper reaches the maximum at a critical grain size of 10 to 15 nm, below which the grain boundary plays a vital role in the nanoscale deformation. The reverse Hall-Petch relation is also confirmed in the uniaxial compression of columnar nanocrystals (see Appendix A). Second, for each polycrystal, the shear stress first increases and then decreases as the impact velocity increases. The maximum Hugoniot shear stress corresponds to the critical impact velocity at HEL. Below the critical impact velocity, the deformation is essentially elastic such that the stress increases with the increase of impact velocity. When the impact velocity exceeds the critical velocity, numerous defects, including dislocations and stacking faults, are generated, which leads to the decrease of shear stress. In addition, the critical impact velocity seems to decrease as the grain size decreases. For the NC copper, the critical velocity is ~500 m/s for the grain size of 10 nm, and it becomes ~400 m/s for the grain sizes of 5 nm and 3 nm. For the SC sample, the critical velocity increases to ~750 m/s which is consistent with the previous study [52]. This variation can be attributed to the reason that for samples with smaller grains, more GBs act as activated sites for the formation of new defects so that the plastic deformation occurs at a relatively lower impact velocity.

3.2. Deformation mechanism around shock Hugoniot

To reveal the shock plasticity, we analyzed the evolution of dislocations in the RVE for the NC copper with a grain size of 5 nm. Since the DXA method [42] can detect the grain boundaries as dislocations [53], we calculated the variation of dislocation densities $\Delta\rho$ to describe the evolution of newly formed dislocations (see Fig. 5(a)). Furthermore, to analyze the stacking faults and twinning, we evaluated the percentages of HCP atoms in the RVE at the Hugoniot state (Fig. 5(b)) because both stacking faults and twinning are arranged in the hexagonal close-packed (HCP) structures. The snapshots of atomic structures at two specific times are illustrated in Fig. 5(c).

For most of the impact velocities in Fig. 5(a), the dislocation density first increases and then remains stable when the shock Hugoniot is achieved in the RVE. Particularly, at the impact velocity of 400 m/s, there is no significant increase in dislocations, and only a few defects can be seen (the yellow arrow) in Fig. 5(c). Therefore, the critical impact velocity at the HEL of NC copper is taken as ~400 m/s, which is consistent with that (~375 m/s) for bicrystals [23]. For the impact strength exceeding the HEL, the dislocation density is the maximum at the impact velocity of 800 m/s ($P_{zz,H}$ = ~ 35 GPa). The defects primarily consist of dislocations below the shock pressure of 35 GPa as observed in the shock experiment of Cu [8]. Since the stacking fault generally forms between the leading and trailing Shockley partial dislocations [54], numerous stacking faults (with two-layered HCP atoms) can also be observed, as shown by the blue arrows in Fig. 5(c).

As the impact velocity exceeds 800 m/s, the dislocation density

decreases as the impact velocity increases, whereas the percentage of HCP atoms keeps increasing, as shown in Fig. 5(b). It is because the primary defect that dominates the shock plasticity changes from dislocation to twinning as the shock pressure increases. The shock experiments [8] revealed that the stacking-fault bundles and twinning are the primary defects at the pressure of 40 GPa; this deformation mechanism is also observed in the simulation. As shown in Fig. 5(c), the nano-twinning with one-layered HCP atoms emerges as marked by the black arrow. For an extremely high impact velocity, such as 1200 m/s ($P_{zz,H} = \sim 58$ GPa), the variation of dislocation density detected by the DXA method first decreases and then keeps increasing. This may be due to two reasons as follows:

1) The defects-induced thermal recovery occurs as reported in [8], which requires more time for stabilization. The dimension of the box cell along the impact direction is not large enough so that dislocations cannot reach a stable state in the RVE at the impact velocity of 1200 m/s. For this high impact velocity, the thermal effect leads to the annihilation of defects on the GB, which reduces the dislocation density initially.
2) The validity of the DXA method depends on the robustness of the atomic structure identification [55], thus the DXA may no longer accurately detect the dislocations when most atoms deviate from the original crystalline structure. Also, as the impact velocity increases to 1200 m/s, the increased thermal effect can reduce the accuracy of atomic structure recognition and then impede the dislocation analysis.

Fig. 5(c) shows an atomic structure transformation from FCC to the body-centered cubic (BCC) at the shock front when $U_p = 1200$ m/s. Subsequently, many of the BCC atoms stabilize in the HCP structure within a short period of time. A similar transition of atomic structures was also observed in [27], which was attributed to the dynamic effect during shock loading.

Interestingly, when the impact velocity reaches ~1000 m/s or higher, it appears that a shielding effect exists within a grain. As shown in Fig. 5(c), once the defect is activated on a slip plane, most of the other defects in the same grain also generate on the parallel slip planes. It is consistent with the defect distribution observed in the multiscale study of the shock-induced plasticity [56]. At the impact velocity as high as ~1000 m/s, numerous defects are generated to release the shear stress to ~1 GPa (see Fig. 4(b)). These defects are confined by the grain boundary, and induce back stress. Lin et al. [57] concluded that the high back stress due to the interactions between dislocations can impede the operation of the second slip system by considering the size-dependent deformation mechanism. Therefore, only a dominant slip system is activated in a grain; the back stress produced by the defects on the parallel slip planes impedes the activation of the other slip systems. In adjacent grains, the defects are activated on other parallel slip planes to achieve deformation compatibility. Li et al. [58] showed that the back stress due to the pile-up of dislocations in a domain would induce a forward stress in the other domain. In our simulation, the back stress in a grain induces forward stress in the neighbor grain such that defects are activated on the other slip planes. For samples subjected to the lower impact velocity/strength, the dislocation density is smaller, and the space between defects is relatively larger. In this case, less plasticity is required to release the external load such that the shielding effect is not obvious.

To clarify the grain size effect on shock plasticity, we further analyzed the defects in the SC copper and the NC copper of different grain sizes at two specific impact velocities, as illustrated in Fig. 6. For the impact velocity of 600 m/s when dislocation dominates the shock plasticity in NC copper, the evolution of dislocations exhibits no clear dependence on the grain size, as shown in Fig. 6(a). The GBs has limited constraint on the evolution of defects because the number of defects is relatively low under the weak impact, see Fig. 5(c). In addition, no defect is observed in the SC copper since the impact strength is below the HEL. As the impact velocity increases to 1000 m/s, the difference in the dislocation densities is apparent due to the effect of grain size, as shown in Fig. 6(b). The dislocation density in the SC copper is much higher than that in the NC copper, and a smaller grain size generally results in fewer dislocations. For this high impact velocity, shock plasticity is produced in all samples. The GB not only acts as a dislocation source but also can absorb dislocations and hinder the dislocation activity. Therefore, the dislocation density is smaller in the sample with more GBs. The shielding effects can be observed in the NC copper with different grain sizes, as shown in Fig. 6(c). In contrast, no dominant slip plane is formed in the SC copper, and defects are widely distributed on different slip planes.

4. Concluding remarks

MD simulations have been performed to investigate the grain size and defect effects on shock plasticity in the columnar NC copper under the impact velocities ranging from 300 m/s to 1200 m/s. The main findings from the study are summarized as below.

1) The shock pressures exhibit no clear dependence on the grain size, and the *P-V* relation matches well with the experimental results available in the open literature. However, the corresponding Hugoniot shear stress depends on the grain size, which is consistent with the grain size dependence of the yield strength under uniaxial compression.
2) As the impact velocity increases, the primary defects transform from dislocation to stacking fault and twinning. The shielding effect is observed in the NC copper, where the defects are formed on the parallel slip planes within a grain. The formation of defects on the parallel slip planes releases the shear stress and increases the back stress so that the activation of other slip systems is suppressed.

CRediT authorship contribution statement

Jianqiao Hu: Conceptualization, Methodology, Investigation, Data curation, Formal analysis, Writing - original draft, Funding acquisition. **Zhen Chen:** Verification, Conceptualization, Writing - review & editing, Supervision.

Declaration of Competing Interest

The authors declare that they have no known competing financial interests or personal relationships that could have appeared to influence the work reported in this paper.

Acknowledgements

The work is supported by the National Natural Science Foundation of China (No. 11802310) and the Science Challenge Project (No. TZ2018001). The authors gratefully acknowledge useful discussions with Prof. Xiaoming Liu from Chinese Academy of Sciences.

Appendix A. SC and NC copper under uniaxial compression

MD simulations under uniaxial compressive loading were performed to clarify the reverse Hall-Petch relation in the NC samples as considered in this study. After the nanocrystals were fabricated by the five-stage procedure presented in section 2, uniaxial compressive loading at a constant strain

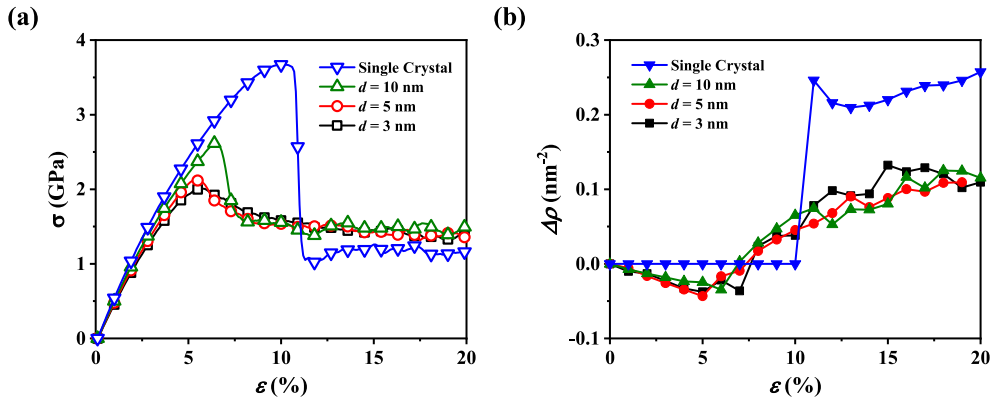

Fig. A1. (a) The stress-strain curves, and (b) the dislocation density-strain curves for SC and NC copper at a strain rate of 5×10^8 s^{-1}.

rate of 5×10^8 s^{-1} was applied in the z-direction (i.e., the column axis) and the global pressure of the sample at the other two lateral directions remained at 0 GPa. All the three directions were periodic during the uniaxial loading. The SC sample was also loaded in the same way. The strain rate effect is not considered here because it was found [32] that the yield stresses of copper with different initial defects exhibit no apparent strain rate sensitivity when the strain rate is below $\sim 10^9$ s^{-1} in the MD simulations.

The stress–strain curves, as well as the evolution of dislocation density, are shown in Fig. A1. The reverse Hall-Petch relation is observed in the NC copper as the incipient yield stress (the peak stress) increases with the increase of grain size. It was interpreted that the dominant deformation mechanism transforms from dislocation-mediated plasticity to GB sliding in the NC metals as the grain size decreases [51]. In Fig. A1(b), the dislocation density initially decreases in the NC copper, which can be attributed to the GB dynamics under external loading. As the loading continues, the dislocation density increases gradually and exhibits no clear grain size dependence. In addition, when the grain size decreases to ~5 nm and below, the yield stress shows little difference. In this case, the grain size decreases towards the width of GB, in which there exist many amorphous atoms. The incipient yield stress in SC copper is much higher due to the homogeneous nucleation of dislocation. After the incipient nucleation of dislocation, the dislocation multiplication prevails and contributes to the plastic deformation. As a result, there exists a dramatic increase in the dislocation density.

Data availability statement

The data that support the findings of this study are available from the corresponding author upon reasonable request.

References

[1] O.E. Jones, J.D. Mote, Shock-induced dynamic yielding in copper single crystals, J. Appl. Phys. 40 (12) (1969) 4920–4928.
[2] B.L. Holian, Modeling shock-wave deformation via molecular dynamics, Phys. Rev. A 37 (7) (1988) 2562–2568.
[3] Q. Johnson, A.C. Mitchell, First X-ray diffraction evidence for a phase transition during shock-wave compression, Phys. Rev. Lett. 29 (20) (1972) 1369–1371.
[4] E. Moshe, S. Eliezer, E. Dekel, A. Ludmirsky, Z. Henis, M. Werdiger, I.B. Goldberg, N. Eliaz, D. Eliezer, An increase of the spall strength in aluminum, copper, and Metglas at strain rates larger than 10^7 s^{-1}, J. Appl. Phys. 83 (8) (1998) 4004–4011.
[5] E. Moshe, S. Eliezer, Z. Henis, M. Werdiger, E. Dekel, Y. Horovitz, S. Maman, I. B. Goldberg, D. Eliezer, Experimental measurements of the strength of metals approaching the theoretical limit predicted by the equation of state, Appl. Phys. Lett. 76 (12) (2000) 1555–1557.
[6] M.S. Schneider, B. Kad, D.H. Kalantar, B.A. Remington, E. Kenik, H. Jarmakani, M. A. Meyers, Laser shock compression of copper and copper–aluminum alloys, Int. J. Impact Eng. 32 (1-4) (2005) 473–507.
[7] G.A. Askaryan, E.M. Moroz, Pressure on evaporation of matter in a radiation beam, J. Exp. Theor. Phys. Lett. 16 (1963) 1638–1644.
[8] M.A. Meyers, F. Gregori, B.K. Kad, M.S. Schneider, D.H. Kalantar, B.A. Remington, G. Ravichandran, T. Boehly, J.S. Wark, Laser-induced shock compression of monocrystalline copper: characterization and analysis, Acta Mater. 51 (5) (2003) 1211–1228.
[9] M.S. Schneider, B.K. Kad, M.A. Meyers, F. Gregori, D. Kalantar, B.A. Remington, Laser-induced shock compression of copper: Orientation and pressure decay effects, Metall. Mater. Trans. A 35 (9) (2004) 2633–2646.
[10] W.D. Turley, S.J. Fensin, R.S. Hixson, D.R. Jones, B.M. La Lone, G.D. Stevens, S. A. Thomas, L.R. Veeser, Spall response of single-crystal copper, J. Appl. Phys. 123 (5) (2018) 055102, https://doi.org/10.1063/1.5012267.
[11] B. Cao, D.H. Lassila, M.S. Schneider, B.K. Kad, C.X. Huang, Y.B. Xu, D.H. Kalantar, B.A. Remington, M.A. Meyers, Effect of shock compression method on the defect substructure in monocrystalline copper, Mater. Sci. Eng. A 409 (1–2) (2005) 270–281.
[12] B.L. Holian, P.S. Lomdahl, Plasticity induced by shock waves in nonequilibrium molecular-dynamics simulations, Science 280 (5372) (1998) 2085–2088.
[13] T.C. Germann, B.L. Holian, P.S. Lomdahl, R. Ravelo, Orientation dependence in molecular dynamics simulations of shocked single crystals, Phys. Rev. Lett. 84 (23) (2000) 5351–5354.
[14] K. Kadau, T.C. Germann, P.S. Lomdahl, B.L. Holian, Microscopic view of structural phase transitions induced by shock waves, Science 296 (2002) 1681–1684.
[15] B. Cao, E.M. Bringa, M.A. Meyers, Shock compression of monocrystalline copper: atomistic simulations, Metall. Mater. Trans. A 38 (11) (2007) 2681–2688.
[16] B. Cao, D.H. Lassila, C. Huang, Y. Xu, M.A. Meyers, Shock compression of monocrystalline copper: experiments, characterization, and analysis, Mater. Sci. Eng. A 527 (3) (2010) 424–434.
[17] D. Tanguy, M. Mareschal, P.S. Lomdahl, T.C. Germann, B.L. Holian, R. Ravelo, Dislocation nucleation induced by a shock wave in a perfect crystal: molecular dynamics simulations and elastic calculations, Phys. Rev. B 68 (14) (2003), 144111.
[18] T.C. Germann, B.L. Holian, P.S. Lomdahl, D. Tanguy, M. Mareschal, R. Ravelo, Dislocation structure behind a shock front in fcc perfect crystals: atomistic simulation results, Metall. Mater. Trans. A 35 (9) (2004) 2609–2615.
[19] M.M. Sichani, D.E. Spearot, A molecular dynamics study of dislocation density generation and plastic relaxation during shock of single crystal Cu, J. Appl. Phys. 120 (4) (2016) 045902, https://doi.org/10.1063/1.4959075.
[20] D. Tramontina, P. Erhart, T. Germann, J. Hawreliak, A. Higginbotham, N. Park, R. Ravelo, A. Stukowski, M. Suggit, Y. Tang, J. Wark, E. Bringa, Molecular dynamics simulations of shock-induced plasticity in tantalum, High Energy Density Phys. 10 (2014) 9–15.
[21] E.N. Hahn, S.J. Fensin, Influence of defects on the shock Hugoniot of tantalum, J. Appl. Phys. 125 (21) (2019) 215902, https://doi.org/10.1063/1.5096526.
[22] T. Hatano, Dislocation nucleation in shocked fcc solids: effects of temperature and preexisting voids, Phys. Rev. Lett. 93 (8) (2004), 085501.
[23] S.-N. Luo, T.C. Germann, D.L. Tonks, Q.i. An, Shock wave loading and spallation of copper bicrystals with asymmetric Σ3⟨110⟩ tilt grain boundaries, J. Appl. Phys. 108 (9) (2010) 093526, https://doi.org/10.1063/1.3506707.
[24] E.M. Bringa, A. Caro, Y. Wang, M. Victoria, J.M. McNaney, B.A. Remington, R. F. Smith, B.R. Torralva, H.V. Swygenhoven, Ultrahigh strength in nanocrystalline materials under shock loading, Science 309 (5742) (2005) 1838–1841.
[25] V. Dremov, A. Petrovtsev, P. Sapozhnikov, M. Smirnova, D.L. Preston, M.A. Zocher, Molecular dynamics simulations of the initial stages of spall in nanocrystalline copper, Phys. Rev. B 74 (14) (2006), 144110.
[26] A.M. Dongare, A.M. Rajendran, B. LaMattina, M.A. Zikry, D.W. Brenner, Atomic scale studies of spall behavior in nanocrystalline Cu, J. Appl. Phys. 108 (11) (2010) 113518, https://doi.org/10.1063/1.3517827.

[27] M.M. Sichani, D.E. Spearot, A molecular dynamics study of the role of grain size and orientation on compression of nanocrystalline Cu during shock, Comput. Mater. Sci. 108 (2015) 226–232.
[28] S.-N. Luo, T.C. Germann, T.G. Desai, D.L. Tonks, Q.i. An, Anisotropic shock response of columnar nanocrystalline Cu, J. Appl. Phys. 107 (12) (2010) 123507, https://doi.org/10.1063/1.3437654.
[29] S. Plimpton, Fast parallel algorithms for short-range molecular dynamics, J. Comput. Phys. 117 (1) (1995) 1–19.
[30] P. Hirel, Atomsk: a tool for manipulating and converting atomic data files, Comput. Phys. Commun. 197 (2015) 212–219.
[31] Y. Mishin, M.J. Mehl, D.A. Papaconstantopoulos, A.F. Voter, J.D. Kress, Structural stability and lattice defects in copper: ab initio, tight-binding, and embedded-atom calculations, Phys. Rev. B 63 (22) (2001), 224106.
[32] J. Hu, X. Ye, X. Liu, Z. Chen, The effects of initial void and dislocation on the onset of plasticity in copper single crystals, J. Appl. Phys. 126 (16) (2019) 165104, https://doi.org/10.1063/1.5125061.
[33] B. Li, L. Wang, J.C. E, H.H. Ma, S.N. Luo, Shock response of He bubbles in single crystal Cu, J. Appl. Phys. 116 (21) (2014) 213506, https://doi.org/10.1063/1.4903732.
[34] P. Wen, G. Tao, C. Pang, S. Yuan, Q. Wang, A molecular dynamics study of the shock-induced defect microstructure in single crystal Cu, Comput. Mater. Sci. 124 (2016) 304–310.
[35] Q. An, S.-N. Luo, L. Li-BoHan, O.T. Zheng, Melting of Cu under hydrostatic and shock wave loading to high pressures, J. Phys.: Condens. Matter 20 (9) (2008) 1–8.
[36] Z.D. Sha, P.S. Branicio, V. Sorkin, Q.X. Pei, Y.W. Zhang, Effects of grain size and temperature on mechanical and failure properties of ultrananocrystalline diamond, Diam. Relat. Mater. 20 (10) (2011) 1303–1309.
[37] C. Huang, X. Peng, B.o. Yang, X. Chen, Q. Li, D. Yin, T. Fu, Effects of strain rate and annealing temperature on tensile properties of nanocrystalline diamond, Carbon 136 (2018) 320–328.
[38] M. Zhou, A new look at the atomic level virial stress: on continuum-molecular system equivalence, proceedings: mathematical, Phys. Eng. Sci. 459 (2037) (2003) 2347–2392.
[39] M.A. Tschopp, D.L. McDowell, Influence of single crystal orientation on homogeneous dislocation nucleation under uniaxial loading, J. Mech. Phys. Solids 56 (5) (2008) 1806–1830.
[40] H. Xie, F. Yin, T. Yu, G. Lu, Y. Zhang, A new strain-rate-induced deformation mechanism of Cu nanowire: transition from dislocation nucleation to phase transformation, Acta Mater. 85 (2015) 191–198.
[41] F. Yuan, X. Wu, Shock response of nanotwinned copper from large-scale molecular dynamics simulations, Phys. Rev. B 86 (13) (2012), 134108.
[42] A. Stukowski, K. Albe, Extracting dislocations and non-dislocation crystal defects from atomistic simulation data, Modell. Simul. Mater. Sci. Eng. 18 (8) (2010) 085001, https://doi.org/10.1088/0965-0393/18/8/085001.
[43] A. Stukowski, Structure identification methods for atomistic simulations of crystalline materials, Modell. Simul. Mater. Sci. Eng. 20 (4) (2012) 045021, https://doi.org/10.1088/0965-0393/20/4/045021.
[44] A. Stukowski, Visualization and analysis of atomistic simulation data with OVITO–the open visualization tool, Modell. Simul. Mater. Sci. Eng. 18 (1) (2010) 015012, https://doi.org/10.1088/0965-0393/18/1/015012.
[45] F. Yuan, L. Chen, P. Jiang, X. Wu, Twin boundary spacing effects on shock response and spall behaviors of hierarchically nanotwinned fcc metals, J. Appl. Phys. 115 (6) (2014) 063509, https://doi.org/10.1063/1.4865738.
[46] S.-N. Luo, Q.i. An, T.C. Germann, L.-B. Han, Shock-induced spall in solid and liquid Cu at extreme strain rates, J. Appl. Phys. 106 (1) (2009) 013502, https://doi.org/10.1063/1.3158062.
[47] M.A. Shehadeh, E.M. Bringa, H.M. Zbib, J.M. McNaney, B.A. Remington, Simulation of shock-induced plasticity including homogeneous and heterogeneous dislocation nucleations, Appl. Phys. Lett. 89 (17) (2006) 171918, https://doi.org/10.1063/1.2364853.
[48] E.M. Bringa, K. Rosolankova, R.E. Rudd, B.A. Remington, J.S. Wark, M. Duchaineau, D.H. Kalantar, J. Hawreliak, J. Belak, Shock deformation of face-centred-cubic metals on subnanosecond timescales, Nat. Mater. 5 (10) (2006) 805–809.
[49] S.P. Marsh, LASL Shock Hugoniot Data, University of California Press, Berkeley, CA, 1980.
[50] M.A. Meyers (Ed.), Dynamic Behavior of Materials, Wiley, 1994.
[51] J. Schiøtz, K.W. Jacobsen, A maximum in the strength of nanocrystalline copper, Science 301 (5638) (2003) 1357–1359.
[52] E.M. Bringa, J.U. Cazamias, P. Erhart, J. Stölken, N. Tanushev, B.D. Wirth, R. E. Rudd, M.J. Caturla, Atomistic shock Hugoniot simulation of single-crystal copper, J. Appl. Phys. 96 (7) (2004) 3793–3799.
[53] B. Kuhr, D. Farkas, Dislocation content in random high angle grain boundaries, Modell. Simul. Mater. Sci. Eng. 27 (4) (2019) 045005, https://doi.org/10.1088/1361-651X/ab122e.
[54] A. Rida, M. Micoulaut, E. Rouhaud, A. Makke, Understanding the strain rate sensitivity of nanocrystalline copper using molecular dynamics simulations, Comput. Mater. Sci. 172 (109294) (2020) 1–9.
[55] A. Stukowski, V.V. Bulatov, A. Arsenlis, Automated identification and indexing of dislocations in crystal interfaces, Modell. Simul. Mater. Sci. Eng. 20 (8) (2012) 085007, https://doi.org/10.1088/0965-0393/20/8/085007.
[56] J. Hu, Z. Liu, K. Chen, Z. Zhuang, Investigations of shock-induced deformation and dislocation mechanism by a multiscale discrete dislocation plasticity model, Comput. Mater. Sci. 131 (2017) 78–85.
[57] P. Lin, Z. Liu, Z. Zhuang, Numerical study of the size-dependent deformation morphology in micropillar compressions by a dislocation-based crystal plasticity model, Int. J. Plast. 87 (2016) 32–47.
[58] X. Li, L. Lu, J. Li, X. Zhang, H. Gao, Mechanical properties and deformation mechanisms of gradient nanostructured metals and alloys, Nat. Rev. Mater. 5 (9) (2020) 706–723.